36. STRUCTURE FUNCTIONS

Written Summer 2001 by B. Foster (Bristol), A.D. Martin (Durham), M.G. Vincter (Alberta).

36.1. Deep inelastic scattering

High energy lepton-nucleon scattering (deep inelastic scattering) plays a key role in determining the partonic structure of the proton. The process $\ell N \to \ell' X$ is illustrated in Fig. 36.1. The filled circle in this figure represents the internal structure of the proton which can be expressed in terms of structure functions.

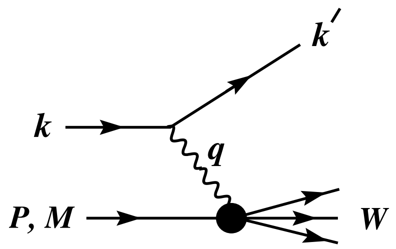

Figure 36.1: Kinematic quantities for the description of deep inelastic scattering. The quantities k and k' are the four-momenta of the incoming and outgoing leptons, P is the four-momentum of a nucleon with mass M, and W is the mass of the recoiling system X. The exchanged particle is a γ, $W^{\pm}$, or Z; it transfers four-momentum $q = k - k'$ to the nucleon.

Invariant quantities:

$\nu = \dfrac{q \cdot P}{M} = E - E'$ is the lepton's energy loss in the nucleon rest frame (in earlier literature sometimes $\nu = q \cdot P$). Here, E and E' are the initial and final lepton energies in the nucleon rest frame.

$Q^2 = -q^2 = 2(EE' - \overrightarrow{k} \cdot \overrightarrow{k}') - m_\ell^2 - m_{\ell'}^2$ where $m_\ell(m_{\ell'})$ is the initial (final) lepton mass. If $EE' \sin^2(\theta/2) \gg m_\ell^2,\, m_{\ell'}^2$, then

$\approx 4EE' \sin^2(\theta/2)$, where θ is the lepton's scattering angle in the nucleon rest frame with respect to the lepton beam direction.

$x = \dfrac{Q^2}{2M\nu}$ where, in the parton model, x is the fraction of the nucleon's momentum carried by the struck quark.

$y = \dfrac{q \cdot P}{k \cdot P} = \dfrac{\nu}{E}$ is the fraction of the lepton's energy lost in the nucleon rest frame.

$W^2 = (P + q)^2 = M^2 + 2M\nu - Q^2$ is the mass squared of the system X recoiling against the scattered lepton.

$s = (k + P)^2 = \dfrac{Q^2}{xy} + M^2 + m_\ell^2$ is the center-of-mass energy squared of the lepton-nucleon system.

The process in Fig. 36.1 is called deep ($Q^2 >> M^2$) inelastic ($W^2 >> M^2$) scattering (DIS). In what follows, the masses of the initial and scattered leptons, m_ℓ and m'_ℓ, are neglected.

36.1.1. ***DIS cross sections***:

$$\frac{d^2\sigma}{dx\,dy} = x\,(s - M^2)\,\frac{d^2\sigma}{dx\,dQ^2} = \frac{2\pi\,M\nu}{E'}\,\frac{d^2\sigma}{d\Omega_{\rm Nrest}\,dE'}\ . \tag{36.1}$$

In lowest order perturbation theory the cross section for the scattering of polarised leptons on polarised nucleons can be expressed in terms of the products of leptonic and hadronic tensors associated with the coupling of the exchanged bosons at the upper and lower vertices in Fig. 36.1 (see Refs. [1,2,3,4])

$$\frac{d^2\sigma}{dxdy} \;=\; \frac{2\pi y\alpha^2}{Q^4}\,\sum_j \eta_j\,L_j^{\mu\nu}\,W_{\mu\nu}^j\ . \tag{36.2}$$

For neutral-current processes the summation is over $j = \gamma, Z$ and γZ representing photon and Z exchange and the interference between them, whereas for charged-current interactions there is only W exchange, $j = W$. (For transverse nucleon polarization there is a dependence on the azimuthal angle of the scattered lepton.) $L_{\mu\nu}$ is the lepton tensor associated with the coupling of the exchange boson to the leptons. For incoming leptons of charge $e = \pm1$ and helicity $\lambda = \pm1$

$$\begin{aligned}
L^\gamma_{\mu\nu} &= 2\left(k_\mu k'_\nu + k'_\mu k_\nu - k\cdot k' g_{\mu\nu} - i\lambda\varepsilon_{\mu\nu\alpha\beta}k^\alpha k'^\beta\right)\\
L^{\gamma Z}_{\mu\nu} &=(g_V^e + e\lambda g_A^e)\;L^\gamma_{\mu\nu}\\
L^{Z}_{\mu\nu} &=(g_V^e + e\lambda g_A^e)^2\;L^\gamma_{\mu\nu}\\
L^{W}_{\mu\nu} &=(1 + e\lambda)^2\;L^\gamma_{\mu\nu}
\end{aligned} \tag{36.3}$$

where

$$g_V^e = -\tfrac{1}{2}\ -\ 2e\sin^2\theta_W, \qquad g_A^e\ =\ -\tfrac{1}{2}\ .$$

Although here the helicity formalism is adopted, an alternative approach is to express the tensors in Eq. (36.3) in terms of the polarization of the lepton.

The factors η_j in Eq. (36.2) denote the ratios of the corresponding propagators and couplings to the photon propagator and coupling squared

$$\begin{aligned}
\eta_\gamma &= 1\\
\eta_{\gamma Z} &= \left(\frac{G_F M_Z^2}{2\sqrt{2}\pi\alpha}\right)\left(\frac{Q^2}{Q^2+M_Z^2}\right)\\
\eta_Z &= \eta^2_{\gamma Z}\\
\eta_W &= \tfrac{1}{2}\left(\frac{G_F M_W^2}{4\pi\alpha}\,\frac{Q^2}{Q^2+M_W^2}\right)^2 .
\end{aligned} \tag{36.4}$$

The hadronic tensor, which describes the interaction of the appropriate electroweak currents with the target nucleon, is given by

$$W_{\mu\nu} = \frac{1}{4\pi} \int d^4z\, e^{iq\cdot z} \left\langle P,S \left| \left[J^\dagger_\mu(z), J_\nu(0) \right] \right| P,S \right\rangle , \qquad (36.5)$$

where S denotes the nucleon-spin 4-vector, with $S^2 = -M^2$ and $S \cdot P = 0$.

36.2. Structure functions of the proton

The structure functions are defined in terms of the hadronic tensor (see Refs. [1,2,3])

$$\begin{aligned}
W_{\mu\nu} = & \left(-g_{\mu\nu} + \frac{q_\mu q_\nu}{q^2} \right) F_1(x,Q^2) + \frac{\hat{P}_\mu \hat{P}_\nu}{P\cdot q} F_2(x,Q^2) \\
& - i\varepsilon_{\mu\nu\alpha\beta} \frac{q^\alpha P^\beta}{2P\cdot q} F_3(x,Q^2) \\
& + i\varepsilon_{\mu\nu\alpha\beta} \frac{q^\alpha}{P\cdot q} \left[S^\beta g_1(x,Q^2) + \left(S^\beta - \frac{S\cdot q}{P\cdot q} P^\beta \right) g_2(x,Q^2) \right] \\
& + \frac{1}{P\cdot q} \left[\tfrac{1}{2} \left(\hat{P}_\mu \hat{S}_\nu + \hat{S}_\mu \hat{P}_\nu \right) - \frac{S\cdot q}{P\cdot q} \hat{P}_\mu \hat{P}_\nu \right] g_3(x,Q^2) \\
& + \frac{S\cdot q}{P\cdot q} \left[\frac{\hat{P}_\mu \hat{P}_\nu}{P\cdot q} g_4(x,Q^2) + \left(-g_{\mu\nu} + \frac{q_\mu q_\nu}{q^2} \right) g_5(x,Q^2) \right] \qquad (36.6)
\end{aligned}$$

where

$$\hat{P}_\mu = P_\mu - \frac{P\cdot q}{q^2} q_\mu , \qquad \hat{S}_\mu = S_\mu - \frac{S\cdot q}{q^2} q_\mu . \qquad (36.7)$$

In Ref. 2 the definition of $W_{\mu\nu}$ with $\mu \leftrightarrow \nu$ is adopted which changes the sign of the $\varepsilon_{\mu\nu\alpha\beta}$ terms in Eq. (36.6), although the formulae given here below are unchanged. Ref. 1 tabulates the relation between the structure functions defined in Eq. (36.6) and other choices available in the literature.

The cross sections for neutral and charged-current deep inelastic scattering on unpolarized nucleons can be written in terms of the structure functions in the generic form

$$\begin{aligned}
\frac{d^2\sigma^i}{dx\,dy} = & \frac{4\pi\alpha^2}{xyQ^2} \eta^i \left\{ \left(1 - y - \frac{x^2y^2M^2}{Q^2} \right) F_2^i \right. \\
& \left. + y^2 x F_1^i \mp \left(y - \frac{y^2}{2} \right) x F_3^i \right\} , \qquad (36.8)
\end{aligned}$$

where i = NC, CC corresponds to neutral-current ($eN \to eX$) or charged-current ($eN \to \nu X$ or $\nu N \to eX$) processes, respectively. In the last term the $-$ sign is taken for an incoming e^+ or $\overline{\nu}$ and the + sign for an incoming e^- or ν. The factor $\eta^{\rm NC} = 1$ for unpolarized $e^\pm$ beams, whereas*

$$\eta^{\rm CC} \;=\; (1 \pm \lambda)^2 \eta_W \tag{36.9}$$

with $\pm$ for $\ell^\pm$ and where λ is the helicity of the incoming lepton. η_W is defined in Eq. (36.4). The CC structure functions, which derive exclusively from W exchange, are

$$F_1^{\rm CC} = F_1^W\,,\; F_2^{\rm CC} = F_2^W\,,\; xF_3^{\rm CC} = xF_3^W\,. \tag{36.10}$$

The NC structure functions $F_2^\gamma, F_2^{\gamma Z}, F_2^Z$ are, for $e^\pm N \to e^\pm X$, given by Ref. 5,

$$F_2^{\rm NC} \;=\; F_2^\gamma \;-\; (g_V^e \pm \lambda g_A^e)\eta_{\gamma Z} F_2^{\gamma Z} \;+\; ({g_V^e}^2 + {g_A^e}^2 \pm 2\lambda g_V^e g_A^e)\;\eta_Z F_2^Z \tag{36.11}$$

and similarly for $F_1^{\rm NC}$, whereas

$$xF_3^{\rm NC} \;=\; -(g_A^e \pm \lambda g_V^e)\eta_{\gamma Z} xF_3^{\gamma Z} + [2g_V^e g_A^e \pm \lambda({g_V^e}^2 + {g_A^e}^2)]\eta_Z xF_3^Z\;. \tag{36.12}$$

The polarized cross-section difference

$$\Delta\sigma \;=\; \sigma(\lambda_n = -1, \lambda_\ell) \;-\; \sigma(\lambda_n = 1, \lambda_\ell)\;, \tag{36.13}$$

where λ_ℓ, λ_n are the helicities (± 1) of the incoming lepton and nucleon, respectively, may be expressed in terms of the five structure functions $g_{1,\ldots 5}(x, Q^2)$ of Eq. (36.6). Thus,

$$\begin{aligned}
\frac{d^2\Delta\sigma^i}{dx\,dy} \;=\; & \frac{8\pi\alpha^2}{xyQ^2}\,\eta^i \left\{ -\lambda_\ell y\left(2 - y - 2x^2y^2\frac{M^2}{Q^2}\right)\, xg_1^i + \lambda_\ell 4x^3y^2\,\frac{M^2}{Q^2}\,g_2^i \right. \\
& + \; 2x^2y\frac{M^2}{Q^2}\left(1 - y - x^2y^2\frac{M^2}{Q^2}\right)\, g_3^i \\
& \left. - \;\left(1 + 2x^2y\frac{M^2}{Q^2}\right)\left[\left(1 - y - x^2y^2\frac{M^2}{Q^2}\right)\, g_4^i + xy^2 g_5^i\right]\right\}
\end{aligned} \tag{36.14}$$

with i = NC or CC as before. The Eq. (36.13) corresponds to the difference of antiparallel minus parallel spins of the incoming particles for e^- or ν initiated reactions, but parallel minus antiparallel for e^+ or $\overline{\nu}$ initiated processes. For longitudinal nucleon polarization, the contributions of g_2 and g_3 are suppressed by powers of M^2/Q^2. These structure functions give an unsuppressed contribution to the cross section for transverse polarization Ref. 1, but in this case the cross-section difference vanishes as $M/Q \to 0$.

Because the same tensor structure occurs in the spin-dependent and spin-independent parts of the hadronic tensor of Eq. (36.6) in the $M^2/Q^2 \to 0$ limit, the differential cross-section difference of Eq. (36.14) may be obtained from the differential cross section Eq. (36.8) by replacing

$$F_1 \to -g_5 \ , \quad F_2 \to -g_4 \ , \quad F_3 \to 2g_1 \ , \tag{36.15}$$

and multiplying by two, since the total cross section is the average over the initial-state polarizations. In this limit Eq. (36.8) and Eq. (36.14) may be written in the form

$$\begin{aligned}
\frac{d^2\sigma^i}{dx\,dy} &= \frac{2\pi\alpha^2}{xyQ^2}\,\eta^i\left[Y_+F_2^i \mp Y_- xF_3^i - y^2 F_L^i\right] \\
\frac{d^2\Delta\sigma^i}{dx\,dy} &= \frac{4\pi\alpha^2}{xyQ^2}\,\eta^i\left[-Y_+g_4^i \mp Y_- 2xg_1^i + y^2 g_L^i\right]
\end{aligned} \tag{36.16}$$

with $i =$ NC or CC, where $Y_\pm = 1 \pm (1-y)^2$ and

$$F_L^i \ = \ F_2^i \ - \ 2xF_1^i \ , \qquad g_L^i \ = \ g_4^i \ - \ 2xg_5^i \ . \tag{36.17}$$

In the naive quark-parton model, the analogy with the Callan-Gross relations [6] $F_L^i = 0$, are the Dicus relations [7] $g_L^i = 0$. Therefore, there are only two independent polarized structure functions: g_1 (parity conserving) and g_5 (parity violating), in analogy to the unpolarized structure functions F_1 and F_3.

36.2.1. *Structure functions in the quark-parton model*:

In the quark-parton model [8,9], contributions to the structure functions F^i and g^i can be expressed in terms of the quark distribution functions $q(x,Q^2)$ of the proton, where $q = u, \overline{u}, d, \overline{d}$ etc. The quantity $q(x,Q^2)dx$ is the number of quarks (or antiquarks) of designated flavor that carry a momentum fraction between x and $x+dx$ of the proton's momentum in a frame in which the proton momentum is large.

For the neutral-current processes $ep \to eX$,

$$\begin{aligned}
\left[F_2^\gamma,\ F_2^{\gamma Z},\ F_2^Z\right] &= x\sum_q\left[e_q^2,\ 2e_qg_V^q,\ g_V^{q\,2}+g_A^{q\,2}\right]\ (q+\overline{q})\ , \\
\left[F_3^\gamma,\ F_3^{\gamma Z},\ F_3^Z\right] &= \sum_q\left[0,\ 2e_qg_A^q,\ 2g_V^qg_A^q\right]\ (q-\overline{q})\ , \\
\left[g_1^\gamma,\ g_1^{\gamma Z},\ g_1^Z\right] &= \tfrac{1}{2}\sum_q\left[e_q^2,\ 2e_qg_V^q,\ g_V^{q\,2}+g_A^{q\,2}\right]\ (\Delta q+\Delta\overline{q})\ , \\
\left[g_5^\gamma,\ g_5^{\gamma Z},\ g_5^Z\right] &= \sum_q\left[0,\ e_qg_A^q,\ g_V^qg_A^q\right]\ (\Delta q-\Delta\overline{q})\ ,
\end{aligned} \tag{36.18}$$

where $g_V^q = \pm\frac{1}{2} - 2e_q\sin^2\theta_W$ and $g_A^q = \pm\frac{1}{2}$ with $\pm$ according to whether q is a $u-$ or $d-$type quark respectively. The quantity Δq is the difference $q\!\uparrow - q\!\downarrow$ of the distributions with the quark spin parallel and antiparallel to the proton spin.

For the charged-current processes $e^- p \to \nu X$ and $\overline{\nu} p \to e^+ X$ the structure functions are:

$$\begin{aligned}
F_2^{W^-} &= 2x(u + \overline{d} + \overline{s} + c \ldots) \, , \\
F_3^{W^-} &= 2(u - \overline{d} - \overline{s} + c \ldots) \, , \\
g_1^{W^-} &= (\Delta u + \Delta\overline{d} + \Delta\overline{s} + \Delta c \ldots) \, , \\
g_5^{W^-} &= (-\Delta u + \Delta\overline{d} + \Delta\overline{s} - \Delta c \ldots) \, ,
\end{aligned} \tag{36.19}$$

where only the active flavors are to be kept and where CKM mixing has been neglected. For $e^+ p \to \overline{\nu} X$ and $\nu p \to e^- X$, the structure functions F^{W^+}, g^{W^+} are obtained by the flavor interchanges $d \leftrightarrow u, s \leftrightarrow c$ in the expressions for F^{W^-}, g^{W^-}. The structure functions for scattering on a neutron are obtained from those of the proton by the interchange $u \leftrightarrow d$. For both the neutral and charged-current processes, the quark-parton model predicts $2xF_1^i = F_2^i$ and $g_4^i = 2xg_5^i$.

Neglecting masses, the structure functions g_2 and g_3 contribute only to scattering from transversely polarized nucleons (for which $S \cdot q = 0$), and have no simple interpretation in terms of the quark-parton model. They arise from off-diagonal matrix elements $\langle P, \lambda' | [J_\mu^\dagger(z), J_\nu(0)] | P, \lambda \rangle$, where the proton helicities satisfy $\lambda' \neq \lambda$. In fact, the leading-twist contributions to both g_2 and g_3 are both twist-2 and twist-3, which contribute at the same order of Q^2 (see the end of Sec. 36.2.2 for a definition of twist) . The Wandzura-Wilczek relation [10] expresses the twist-2 part of g_2 in terms of g_1

$$g_2^i(x) \;=\; -g_1^i(x) \;+\; \int_x^1 \frac{dy}{y}\, g_1^i(y) \; . \tag{36.20}$$

However the twist-3 component of g_2 is unknown. Similarly there is a relation expressing the twist-2 part of g_3 in terms of g_4. A complete set of relations, including M^2/Q^2 effects, can be found in Ref. 11.

36.2.2. *Structure functions and QCD*:

One of the most striking predictions of the quark-parton model is that the structure functions F^i, g^i *scale, i.e.*, $F^i(x, Q^2) \to F^i(x)$ in the Bjorken limit that Q^2 and $\nu \to \infty$ with x fixed [12]. This property is related to the assumption that the transverse momentum of the partons in the infinite-momentum frame of the proton is small. In QCD, however, the radiation of hard gluons from the quarks violates this assumption, leading to logarithmic scaling violations. The radiation of gluons produces the evolution of both the structure functions and the parton distribution functions. As Q^2 increases, more and more gluons are radiated, which in turn split into $q\overline{q}$ pairs. This process leads both to the softening of the initial quark momentum distributions and to the growth of the gluon density and the $q\overline{q}$ sea as x decreases. The effects of the Q^2 evolution can be seen in Fig. 36.2, where F_2 is plotted at two values of Q^2.

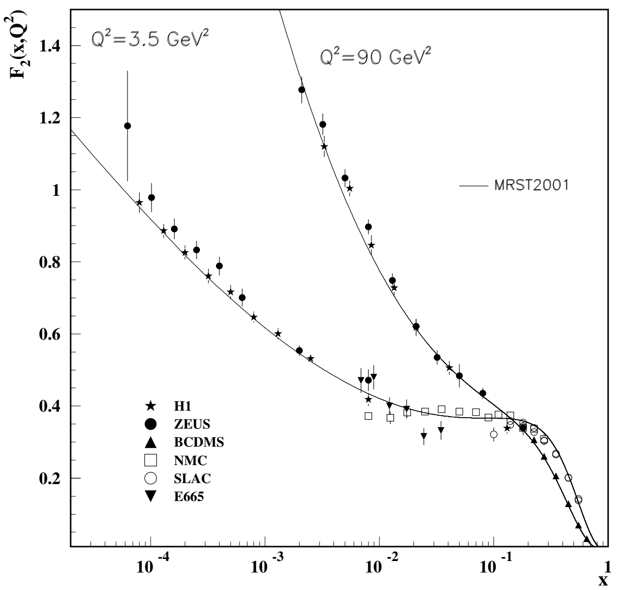

Figure 36.2: The proton structure function F_2^p given at two Q^2 values (3.5 GeV^2 and 90 GeV^2), which exhibit scaling at the 'pivot' point $x \sim 0.14$. See the caption in Fig. 36.6 for the references of the data. Also shown is the MRST2001 parameterization [13] given at the same scales.

In QCD, the above process is described in terms of scale-dependent parton distributions $f(x, \mu^2)$, where $f = g$ or q and, typically, μ is the scale of the probe Q. These distributions correspond, at a given x, to the density of partons in the proton integrated over transverse momentum k_t up to μ. Their evolution in μ is described in QCD by the DGLAP equations (see Refs. [14,15,16,17]) which have the schematic form

$$\frac{\partial f}{\partial \ln \mu^2} \sim \frac{\alpha_s(\mu^2)}{2\pi} (P \otimes f) \ , \tag{36.21}$$

where $\otimes$ denotes the convolution integral

$$P \otimes f = \int_x^1 \frac{dy}{y} P(y) \, f\left(\frac{x}{y}\right) \ . \tag{36.22}$$

Although perturbative QCD can predict, via Eq. (36.21), the evolution of the parton distribution functions from a particular scale, μ_0, it cannot predict them *a priori* at any particular μ_0. Thus they must be measured at a starting point μ_0 before the predictions of QCD can be compared to the data at other scales, μ. In general, all observables involving a hard hadronic interaction (such as structure functions) can be expressed as a convolution of calculable, process-dependent coefficient functions and these universal parton distributions.

It is often convenient to write the evolution equations in terms of the gluon, non-singlet (q^{NS}) and singlet (q^S) quark distributions, such that

$$q^{NS} = q_i - \overline{q}_i, \qquad q^S = \sum_i (q_i + \overline{q}_i) \ . \tag{36.23}$$

The non-singlet distributions have non-zero values of flavor quantum numbers, such as isospin and baryon number. The DGLAP evolution equations then take the form

$$\begin{aligned} \frac{\partial q^{NS}}{\partial \ln \mu^2} &= \frac{\alpha_s(\mu^2)}{2\pi} P_{qq} \otimes q^{NS} \ , \\ \frac{\partial}{\partial \ln \mu^2} \begin{pmatrix} q^S \\ g \end{pmatrix} &= \frac{\alpha_s(\mu^2)}{2\pi} \begin{pmatrix} P_{qq} & 2n_f \, P_{qg} \\ P_{gq} & P_{gg} \end{pmatrix} \otimes \begin{pmatrix} q^S \\ g \end{pmatrix} \ , \end{aligned} \tag{36.24}$$

where P are splitting functions that describe the probability of a given parton splitting into two others, and n_f is the number of (active) quark flavors. The leading-order Altarelli-Parisi [16] splitting functions are

$$P_{qq} = \frac{4}{3} \left[\frac{1+x^2}{(1-x)} \right]_+ = \frac{4}{3} \left[\frac{1+x^2}{(1-x)_+} \right] + 2\delta(1-x) \ , \tag{36.25}$$

$$P_{qg} = \frac{1}{2} \left[x^2 + (1-x)^2 \right] \ , \tag{36.26}$$

$$P_{gq} = \frac{4}{3} \left[\frac{1+(1-x)^2}{x} \right] \ , \tag{36.27}$$

$$\begin{aligned} P_{gg} = 6 &\left[\frac{1-x}{x} + x(1-x) + \frac{x}{(1-x)_+} \right] \\ &+ \left[\frac{11}{2} - \frac{n_f}{3} \right] \delta(1-x), \end{aligned} \tag{36.28}$$

where the notation $[F(x)]_+$ defines a distribution such that for any sufficiently regular test function $f(x)$

$$\int_0^1 dx f(x)[F(x)]_+ = \int_0^1 dx \ (f(x) - f(1))F(x) \ . \tag{36.29}$$

In general, the structure functions can be expressed as a power series in α_s. The series contains both terms proportional to $\ln \mu^2$ and to $\ln 1/x$. The leading $\ln \mu^2$ terms come, in an axial gauge, from evolution along the parton chain which is strongly ordered in transverse momenta, that is $\mu^2 \gg k_{t,n}^2 \gg k_{t,n-1}^2 \gg \ldots$, where n denotes the n^{th} parton-branching process and k_t the parton transverse momentum. The leading-order

DGLAP evolution sums up the $(\alpha_s \ln \mu^2)^n$ contributions. The next-to-leading order (NLO) sums up the $\alpha_s(\alpha_s \ln \mu^2)^{n-1}$ terms [18,19], which arise when two adjacent $k_{t,i}$'s are no longer strongly ordered but become comparable, thereby losing a factor of $\ln \mu^2$. The NNLO contributions are now almost all known [20,21].

In the small x kinematic region it is essential to sum leading terms in $\ln 1/x$, independent of the value of $\ln \mu^2$. At leading order, this is done by the BFKL equation for the unintegrated distributions (see Refs. [22,23]). The leading-order $(\alpha_s \ln(1/x))^n$ terms come from the configuration strongly ordered in x, *i.e.*, $x \ll x_n \ll x_{n-1} \ll \ldots$.

In general, however, QCD color coherence implies *angular* ordering along the chain, so that it is necessary to work in terms of $f_a(x, k_t^2, \mu^2)$, the parton distributions unintegrated over k_t. These distributions depend on two hard scales: k_t and the scale μ of the probe. Consequently they satisfy more complicated CCFM evolution equations [24,25]. The DGLAP and BFKL equations are two limits of angular-ordered evolution. In the DGLAP collinear approximation, the angle increases due to the growth of k_t, while, in the BFKL treatment, the angle ($\theta \simeq k_t/k_l$, where k_l is the longitudinal momentum) grows due to the decrease of the longitudinal-momentum fraction, x, along the chain of parton emissions from the proton.

As yet, there is no firm evidence in the data for $Q^2 \gtrsim 2$ GeV^2 for any deviation from standard DGLAP evolution, except that some DGLAP parton sets predict an unphysical behavior for F_L at low x [13].

The precision of the contemporary experimental data demands that NLO (or even NNLO) DGLAP evolution be used in comparisons between QCD theory and experiment. At higher orders, it is necessary to specify, and to use consistently, both a renormalization and a factorization scheme. Whereas the renormalization scheme used is almost universally the modified minimal subtraction ($\overline{MS}$) scheme, there are two popular choices for factorization scheme, in which the form of the correction for each structure function is different. The two most-used factorization schemes are: DIS [26], in which there are no higher-order corrections to the F_2 structure function, and $\overline{MS}$ (based on Refs. [27,28,29]). They differ by how the higher-order gluon divergences are assimilated in the parton distribution functions.

Perturbative QCD predicts the Q^2 behavior of leading-twist (twist-2) contributions to the structure functions. Higher-twist terms, which involve their own non-perturbative input, can occur. These die off as powers of Q; specifically twist-n terms are damped by $1/Q^{n-2}$. The higher-twist terms appear to be numerically unimportant for Q^2 above a few GeV^2, except for x close to 1. At very large values of x, perturbative corrections proportional to $\log(1-x)$ can become important [30].

So far, it has been assumed that the quarks are massless. The effects of the c and b quark masses on the evolution have been studied in Refs. 31–37. A variable flavor number approach is now generally adopted, in which evolution with $n_f = 3$ is matched to that with $n_f = 4$ at the charm threshold, with an analogous matching at the bottom threshold.

36.3. Determination of parton distributions

The parton distribution functions (PDFs) can be determined from data for deep inelastic lepton-nucleon scattering and for related hard-scattering processes initiated by nucleons. Table 36.1 given below (based on Ref. 38) highlights some processes and their primary sensitivity to PDFs.

Table 36.1: Lepton-nucleon and related hard-scattering processes and their primary sensitivity to the parton distributions that are probed.

Process	Main Subprocess	PDFs Probed
$\ell^{\pm}N \to \ell^{\pm}X$	$\gamma^* q \to q$	$g(x \lesssim 0.01), q, \overline{q}$
$\ell^+(\ell^-)N \to \overline{\nu}(\nu)X$	$W^* q \to q'$	
$\nu(\overline{\nu})N \to \ell^-(\ell^+)X$	$W^* q \to q'$	
$\nu\, N \to \mu^+\mu^- X$	$W^* s \to c \to \mu^+$	s
$pp \to \gamma X$	$qg \to \gamma q$	$g(x \sim 0.4)$
$pN \to \mu^+\mu^- X$	$q\overline{q} \to \gamma^*$	$\overline{q}$
$pp, pn \to \mu^+\mu^- X$	$u\overline{u}, d\overline{d} \to \gamma^*$	$\overline{u} - \overline{d}$
	$u\overline{d}, d\overline{u} \to \gamma^*$	
$ep, en \to e\pi X$	$\gamma^* q \to q$	
$p\overline{p} \to W \to \ell^{\pm}X$	$ud \to W$	$u, d, u/d$
$p\overline{p} \to$ jet $+X$	$gg, qg, qq \to 2j$	$q, g(0.01 \lesssim x \lesssim 0.5)$

The kinematic ranges of fixed-target and collider experiments are complementary (as is shown in Fig. 36.3) which enables the determination of PDFs over a wide range in x and Q^2. The unpolarized PDFs are determined through next-to-leading order global analyses of experimental data from such processes as those listed in the table above. See for example Refs. [13,39,40] for more detailed discussions of such global analyses. The result of one analysis is shown in Fig. 36.4 at a scale $\mu^2 = 10$ GeV^2. The polarized PDFs are obtained through NLO global analyses of measurements of the g_1 structure function in inclusive polarized deep inelastic scattering (see for example Refs. 41,42). The inclusive data do not provide enough observables to determine all polarized PDFs. These polarized PDFs may be fully accessed via flavor tagging in semi-inclusive deep inelastic scattering. Fig. 36.5 shows one global analysis at a scale of 2.5 GeV^2 along with the data from semi-inclusive DIS.

Comprehensive sets of PDFs available as program-callable functions can be obtained from several sources *e.g.*, Refs. 45,46.

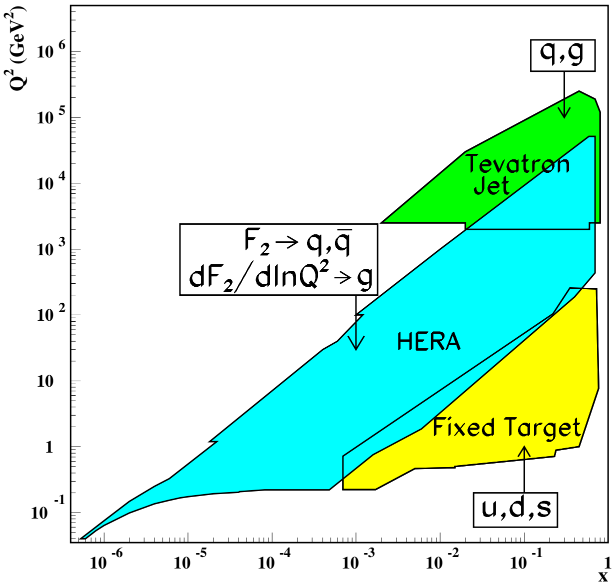

Figure 36.3: Kinematic domains in x and Q^2 probed by fixed-target and collider experiments, shown together with the important constraints they make on the various parton distributions.

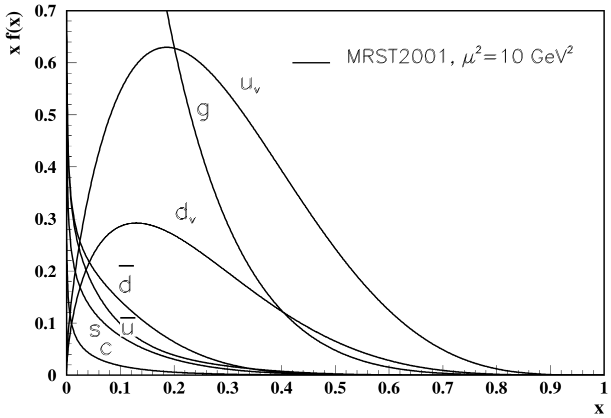

Figure 36.4: Distributions of x times the unpolarized parton distributions $f(x)$ (where $f = u_v, d_v, \overline{u}, \overline{d}, s, c, g$) using the MRST2001 parameterization [13] at a scale $\mu^2 = 10$ GeV^2.

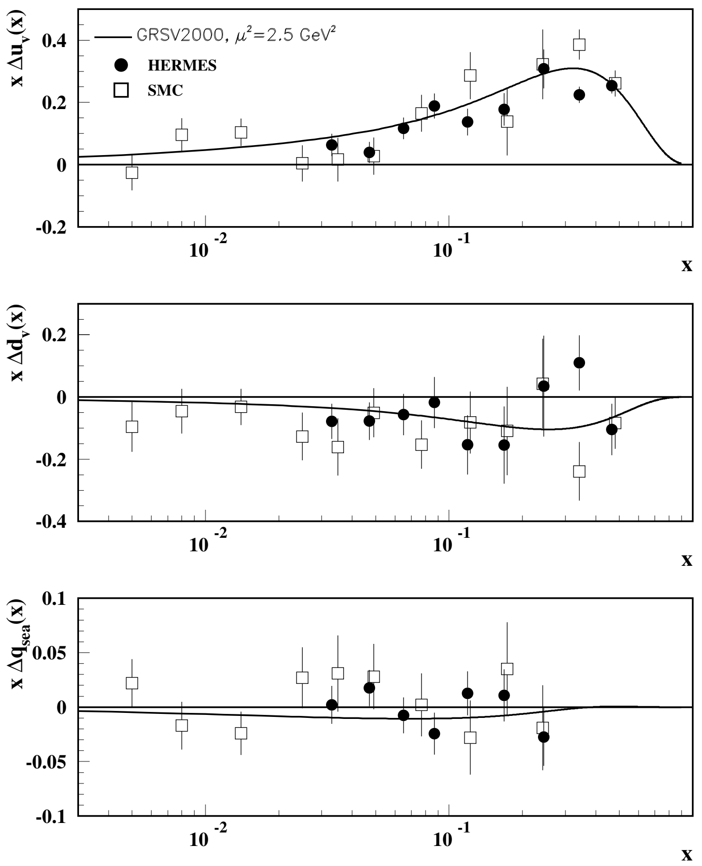

Figure 36.5: Distributions of x times the polarized parton distributions $\Delta q(x)$ (where $q = u_v, d_v, q_{sea}$) using the GRSV2000 parameterization [42] at a scale $\mu^2 = 2.5$ GeV^2. Points represent data from semi-inclusive positron (HERMES [43]) and muon (SMC [44]) deep inelastic scattering given at $Q^2 = 2.5$ GeV^2.

36.4. DIS determinations of α_s

In the fits to the DIS data, $\alpha_s(M_Z^2)$ is often left as a free parameter. For example, a recent NLO DGLAP fit by H1 [47] to their F_2 measurements, together with those of BCDMS, gives

$$\alpha_s(M_Z^2) = 0.1150 \pm 0.0017(\mathrm{expt})^{+0.0009}_{-0.0005}(\mathrm{model}) \pm 0.005(\mathrm{theory}). \tag{36.30}$$

There is a strong correlation between the value found for α_s and the behavior of the gluon distribution. A NLO global analysis [13] which includes all the latest unpolarized DIS data, together with recent Tevatron jet data to constrain the large x gluon distribution, finds

$$\alpha_s(M_Z^2) = 0.119 \pm 0.002(\mathrm{expt}) \pm 0.003(\mathrm{theory}). \tag{36.31}$$

Interestingly, even if the jet data were omitted in this global fit, result Eq. (36.31) is still obtained.

There have been several studies of α_s at NNLO, and beyond, using subsets of DIS data (see Refs. 48–51). Moreover there exist global NLO analyses of polarised DIS data which give $\alpha_s(M_Z^2) = 0.120 \pm 0.009$ [52] and 0.114 ± 0.009 [53].

---

* The value of η^{CC} deduced from Ref. 1 is found to be a factor of two too small; η^{CC} of Eq. (36.9) agrees with Refs. 2,3.

References:

1. J. Blümlein and N. Kochelev, Nucl. Phys. **B498**, 285 (1997).
2. S. Forte, M.L. Mangano, and G. Ridolfi, Nucl. Phys. **B602**, 585 (2001).
3. M. Anselmino, P. Gambino, and J. Kalinowski, Z. Phys. **C64**, 267 (1994).
4. M. Anselmino, A. Efremov, and E. Leader, Phys. Rep. **261**, 1 (1995).
5. M. Klein and T. Riemann, Z. Phys. **C24**, 151 (1984).
6. C.G. Callan and D.J. Gross, Phys. Rev. Lett. **22**, 156 (1969).
7. D.A. Dicus, Phys. Rev. **D5**, 1367 (1972).
8. J.D. Bjorken and E.A. Paschos, Phys. Rev. **185**, 1975 (1969).
9. R.P. Feynman, Photon Hadron Interactions (Benjamin, New York, 1972).
10. S. Wandzura and F. Wilczek, Phys. Rev. **B72**, 195 (1977).
11. J. Blümlein and A. Tkabladze, Nucl. Phys. **B553**, 427 (1999).
12. J.D. Bjorken, Phys. Rev. **179**, 1547 (1969).
13. A.D. Martin, R.G. Roberts, W.J. Stirling, and R.S. Thorne, `hep-ph/0110215`.
14. V.N. Gribov and L.N. Lipatov, Sov. J. Nucl. Phys. **15**, 438 (1972).
15. L.N. Lipatov, Sov. J. Nucl. Phys. **20**, 95 (1975).
16. G. Altarelli and G. Parisi, Nucl. Phys. **B126**, 298 (1977).
17. Yu.L. Dokshitzer, Sov. Phys. JETP **46**, 641 (1977).
18. G. Curci, W. Furmanski, and R. Petronzio, Nucl. Phys. **B175**, 27 (1980).
19. R.K. Ellis, W.J. Stirling, and B.R. Webber, QCD and Collider Physics (Cambridge UP, 1996).
20. S. Moch and J. Versmaseren, Nucl. Phys. **B573**, 853 (2000).
21. A. Retey and J. Versmaseren, Nucl. Phys. **B604**, 281 (2001).
22. E.A. Kuraev, L.N. Lipatov, and V.S. Fadin, Phys. Lett. **B60**, 50 (1975); Sov. Phys. JETP **44**, 443 (1976); Sov. Phys. JETP **45**, 199 (1977).
23. Ya.Ya. Balitsky and L.N. Lipatov, Sov. J. Nucl. Phys. **28**, 822 (1978).
24. M. Ciafaloni, Nucl. Phys. **B296**, 49 (1988).
25. S. Catani, F. Fiorani, and G. Marchesini, Phys. Lett. **B234**, 339 (1990); Nucl. Phys. **B336**, 18 (1990).
26. G. Altarelli, R.K. Ellis, and G. Martinelli, Nucl. Phys. **B143**, 521 (1978) and erratum: Nucl. Phys. **B146**, 544 (1978).
27. G. 't Hooft and M. Veltman, Nucl. Phys. **B44**, 189 (1972).
28. G. 't Hooft, Nucl. Phys. **B61**, 455 (1973).
29. W.A. Bardeen *et al.*, Phys. Rev. **D18**, 3998 (1978).
30. G. Sterman, Nucl. Phys. **B281**, 310 (1987).
31. M.A.G. Aivazis *et al.*, Phys. Rev. **D50**, 3102 (1994).
32. J.C. Collins, Phys. Rev. **D58**, 094002 (1998).
33. A.D. Martin *et al.*, Eur. Phys. J. **C2**, 287 (1998).

34. B.W. Harris and J. Smith, Phys. Rev. **D57**, 2806 (1998); Nucl. Phys. **B452**, 109 (1995); Phys. Lett. **B353**, 535 (1995).
35. A. Chuvakin, J. Smith, and W.L. van Neerven, Phys. Rev. **D6**, 096004 (2000); Phys. Rev. **D62**, 036004 (2000).
36. E. Laenan *et al.*, Nucl. Phys. **B392**, 162 (1993); Nucl. Phys. **B392**, 229 (1993).
37. R.S. Thorne and R.G. Roberts, Phys. Rev. **D57**, 1998 (1998); Phys. Lett. **B421**, 303 (1998); Eur. Phys. J. **C19**, 339 (2001).
38. A.D. Martin, R.G. Roberts, W.J. Stirling, and R.S. Thorne, Eur. Phys. J. **C4**, 463 (1998).
39. M. Glück, E. Reya, and A. Vogt, Eur. Phys. J. **C5**, 461 (1998).
40. H.L. Lai *et al.*, Eur. Phys. J. **C12**, 375 (2000).
41. T. Gehrmann and W.J. Stirling, Phys. Rev. **D53**, 6100 (1996).
42. M. Glück, E. Reya, M. Stratmann, and W. Vogelsang, Phys. Rev. **D63**, 094005 (2001).
43. HERMES, K. Ackerstaff *et al.*, Phys. Lett. **B464**, 123 (1999).
44. SMC, B. Adeva *et al.*, Phys. Lett. **B420**, 180 (1998).
45. H. Plothow-Besch, Comp. Phys. Comm. **75**, 396 (1993).
46. `http://durpdg.dur.ac.uk/HEPDATA/PDF`.
47. H1, C. Adloff *et al.*, Eur. Phys. J. **C21**, 33 (2001).
48. W.L. van Neerven and A. Vogt, Nucl. Phys. **B603**, 42 (2001).
49. J. Santiago and F.J. Yndurain, Nucl. Phys. **B611**, 447 (2001).
50. A.L. Kataev, G. Parente, and A.V. Sidorov, `hep-ph/0106221`.
51. S. Alekhin, Phys. Lett. **B519**, 57 (2001).
52. G. Altarelli, R.D. Ball, S. Forte, and G. Ridolfi, Nucl. Phys. **B496**, 337 (1997).
53. J. Blümlein and H. Böttcher, `hep-ph/0107317`.

NOTE: THE FIGURES IN THIS SECTION ARE INTENDED TO SHOW THE REPRESENTATIVE DATA. THEY ARE NOT MEANT TO BE COMPLETE COMPILATIONS OF ALL THE WORLD'S RELIABLE DATA.

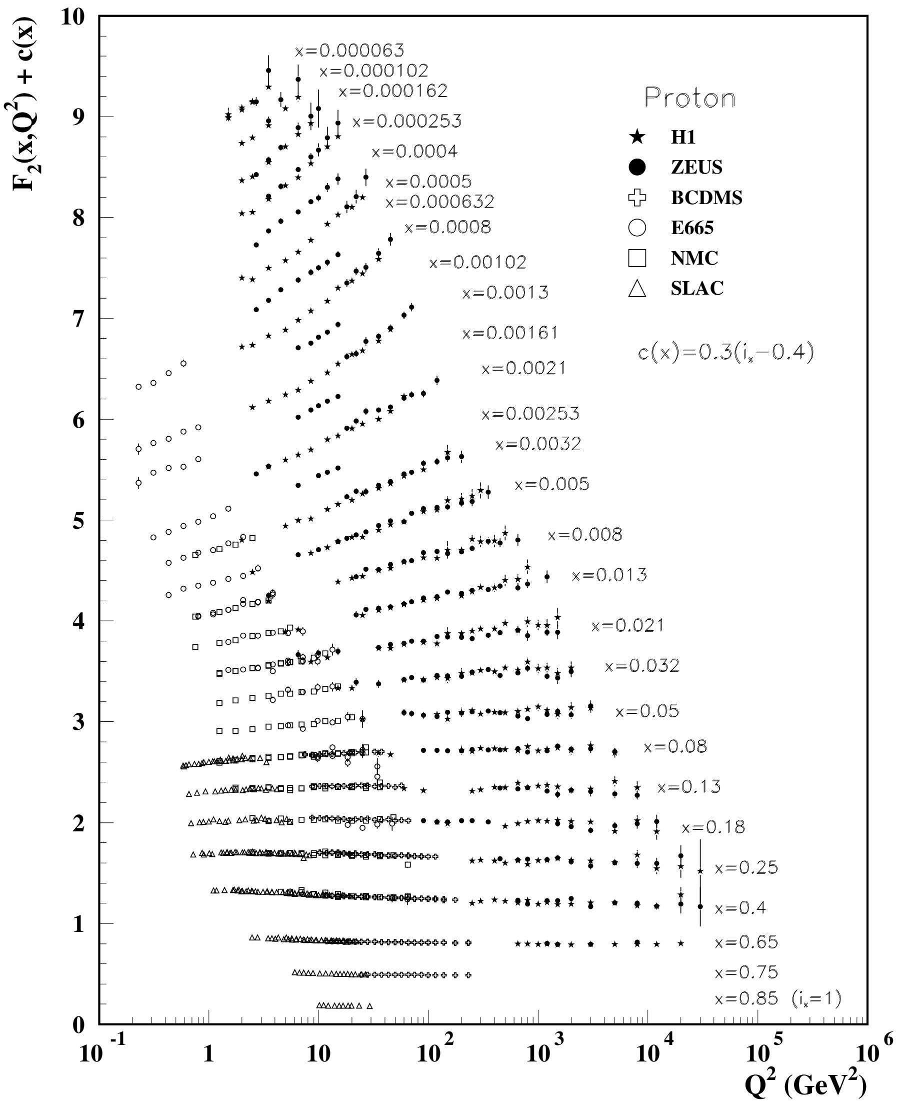

Figure 36.6: The proton structure function F_2^p measured in electromagnetic scattering of positrons on protons (collider experiments ZEUS and H1), in the kinematic domain of the HERA data, for $x > 0.00006$ (*cf.* Fig. 36.9 for data at smaller x and Q^2), and for electrons (SLAC) and muons (BCDMS, E665, NMC) on a fixed target. Statistical and systematic errors added in quadrature are shown. The data are plotted as a function of Q^2 in bins of fixed x. The ZEUS binning in x is used in this plot; all other data are rebinned to the x values of the ZEUS data. For the purpose of plotting, a constant $c(x) = 0.3(i_x - 0.4)$ is added to F_2^p, where i_x is the number of the x bin ranging from $i_x = 1$ ($x = 0.85$) to $i_x = 28$ ($x = 0.000063$). References: **H1**— C. Adloff *et al.*, Eur. Phys. J. **C21**, 33 (2001); C. Adloff *et al.*, Eur. Phys. J. **C13**, 609 (2000); **ZEUS**—S. Chekanov *et al.*, Eur. Phys. J. **C21**, 443 (2001); **BCDMS**—A.C. Benvenuti *et al.*, Phys. Lett. **B223**, 485 (1989) (as given in [46]); **E665**—M.R. Adams *et al.*, Phys. Rev. **D54**, 3006 (1996); **NMC**—M. Arneodo *et al.*, Nucl. Phys. **B483**, 3 (97); **SLAC**—L.W. Whitlow *et al.*, Phys. Lett. **B282**, 475 (1992).

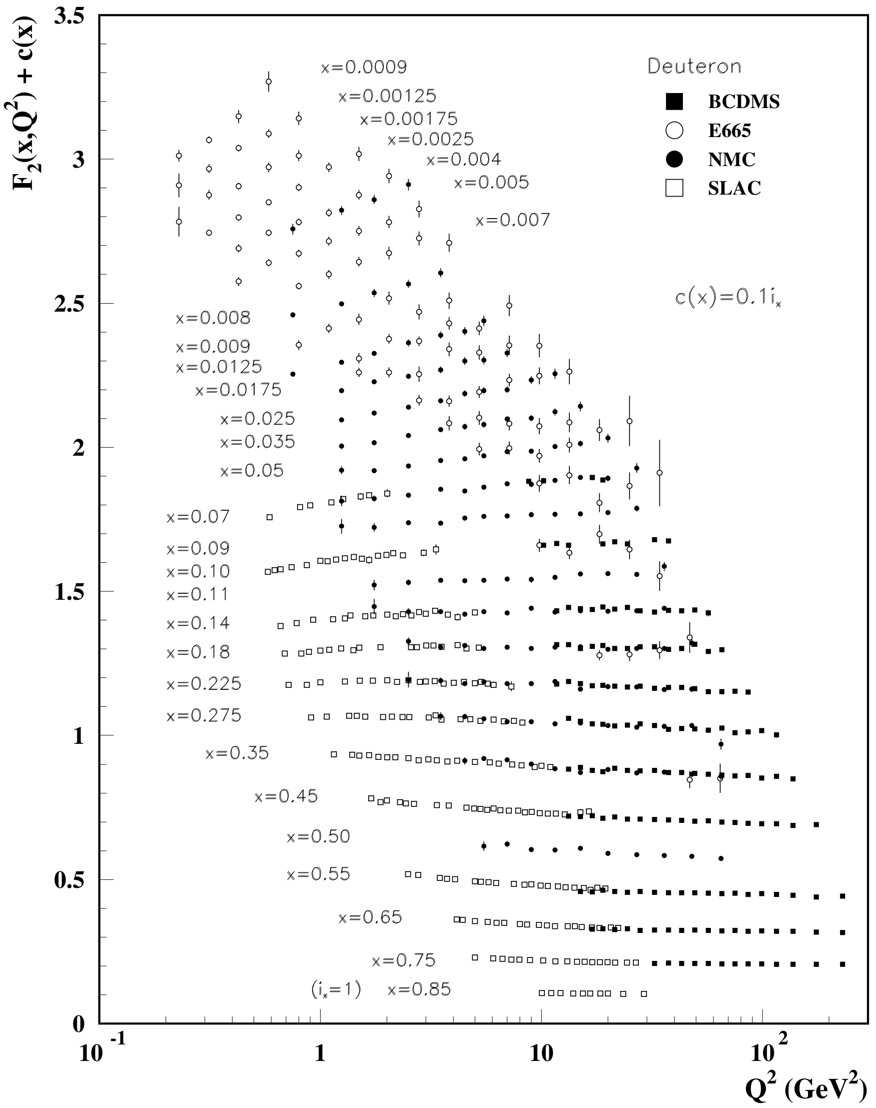

Figure 36.7: The deuteron structure function F_2^d measured in electromagnetic scattering of electrons (SLAC) and muons (BCDMS, E665, NMC) on a fixed target, shown as a function of Q^2 for bins of fixed x. Statistical and systematic errors added in quadrature are shown. For the purpose of plotting, a constant $c(x) = 0.1 i_x$ is added to F_2^p where i_x is the number of the x bin, ranging from 1 ($x = 0.85$) to 29 ($x = 0.0009$). References: **BCDMS**—A.C. Benvenuti *et al.*, Phys. Lett. **B237**, 592 (1990). **E665, NMC, SLAC**—same references as Fig. 36.6.

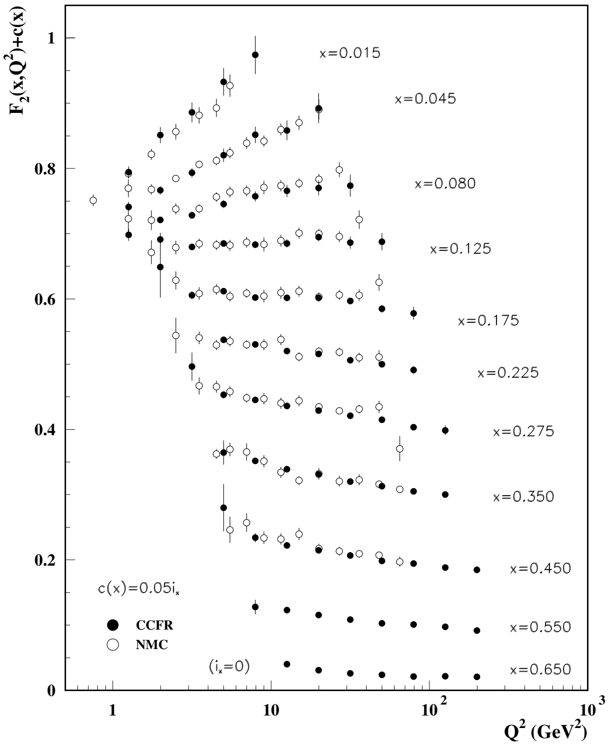

Figure 36.8: The deuteron structure function F_2 measured in deep inelastic scattering of muons on a fixed target (NMC) is compared to the structure function F_2 from neutrino-iron scattering (CCFR) using $F_2^\mu = (5/18)F_2^\nu - x(s+\overline{s})/6$, where heavy target effects have been taken into account. The data are shown versus Q^2, for bins of fixed x. The NMC data have been rebinned to CCFR x values. Statistical and systematic errors added in quadrature are shown. For the purpose of plotting, a constant $c(x) = 0.05i_x$ is added to F_2 where i_x is the number of the x bin, ranging from 0 ($x = 0.65$) to 10 ($x = 0.015$). References: **NMC**—M. Arneodo *et al.*, Nucl. Phys. **B483**, 3 (97); **CCFR/NuTeV**—U.K. Yang *et al.*, Phys. Rev. Lett. **86**, 2741 (2001).

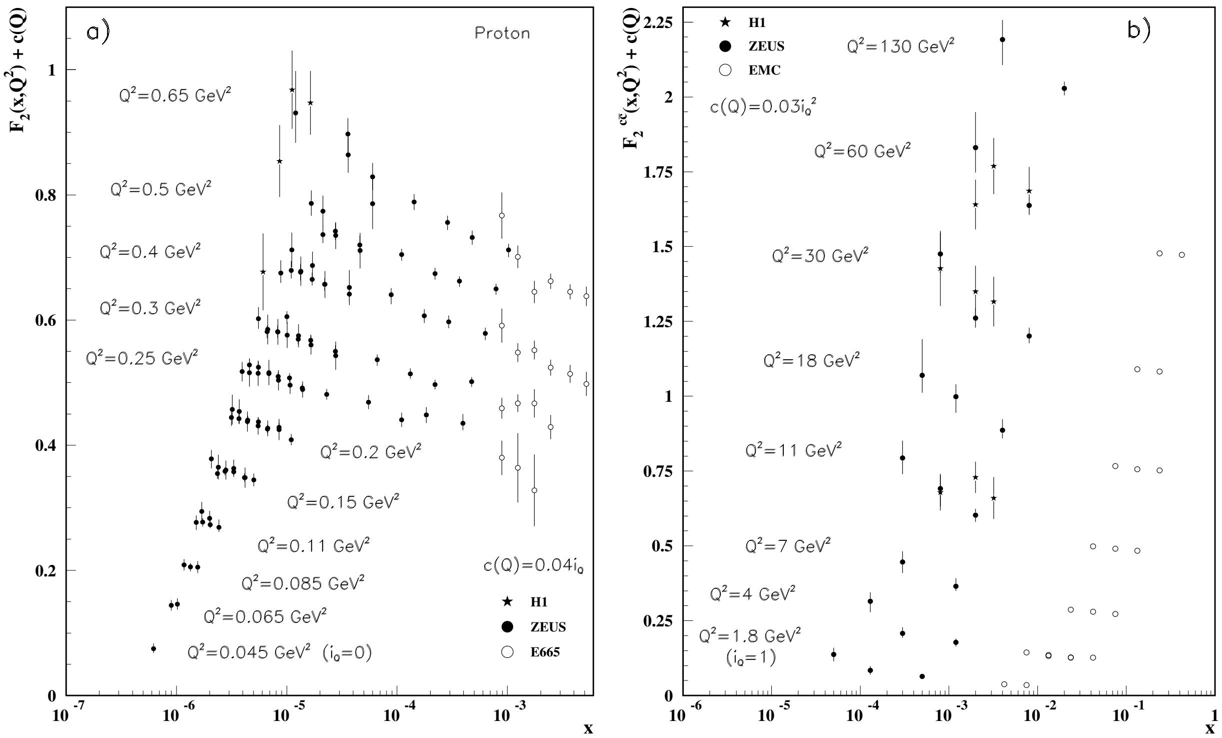

Figure 36.9: a) The proton structure function F_2^p at small x and Q^2, measured in electromagnetic scattering of positrons (H1, ZEUS) and muons (E665) on protons. For the purpose of plotting, a constant $c(Q) = 0.04 i_Q$ is added to F_2^p where i_Q is the number of the Q^2 bin, ranging from 0 ($Q^2 = 0.045$ GeV^2) to 10 ($Q^2 = 0.65$ GeV^2). References: **ZEUS**—J. Breitweg *et al.*, Phys. Lett. **B407**, 432 (1997); J. Breitweg *et al.*, Phys. Lett. **B487**, 53 (2000); J. Breitweg *et al.*, Eur. Phys. J. **C7**, 609 (1999); **H1**—C. Adloff *et al.*, Nucl. Phys. **B497**, 3 (1997); **E665**—M.R. Adams *et al.*, Phys. Rev. **D54**, 3006 (1996).

b) The charm structure function $F_2^{c\overline{c}}(x)$, i.e. that part of the inclusive structure function F_2^p arising from the production of charm quarks, measured in electromagnetic scattering of positrons on protons (H1, ZEUS) and muons on iron (EMC). For the purpose of plotting, a constant $c(Q) = 0.03 i_Q^2$ is added to $F_2^{c\overline{c}}$ where i_Q is the number of the Q^2 bin, ranging from 1 ($Q^2 = 1.8$ GeV^2) to 8 ($Q^2 = 130$ GeV^2). References: **ZEUS**—J. Breitweg *et al.*, Eur. Phys. J. **C12**, 35 (2000); **H1**—C. Adloff *et al.*, Z. Phys. **C72**, 593 (1996); **EMC**—J.J. Aubert *et al.*, Nucl. Phys. **B213**, 31 (1983).

Statistical and systematic errors added in quadrature are shown for both plots. The data are given as a function of x in bins of Q^2.

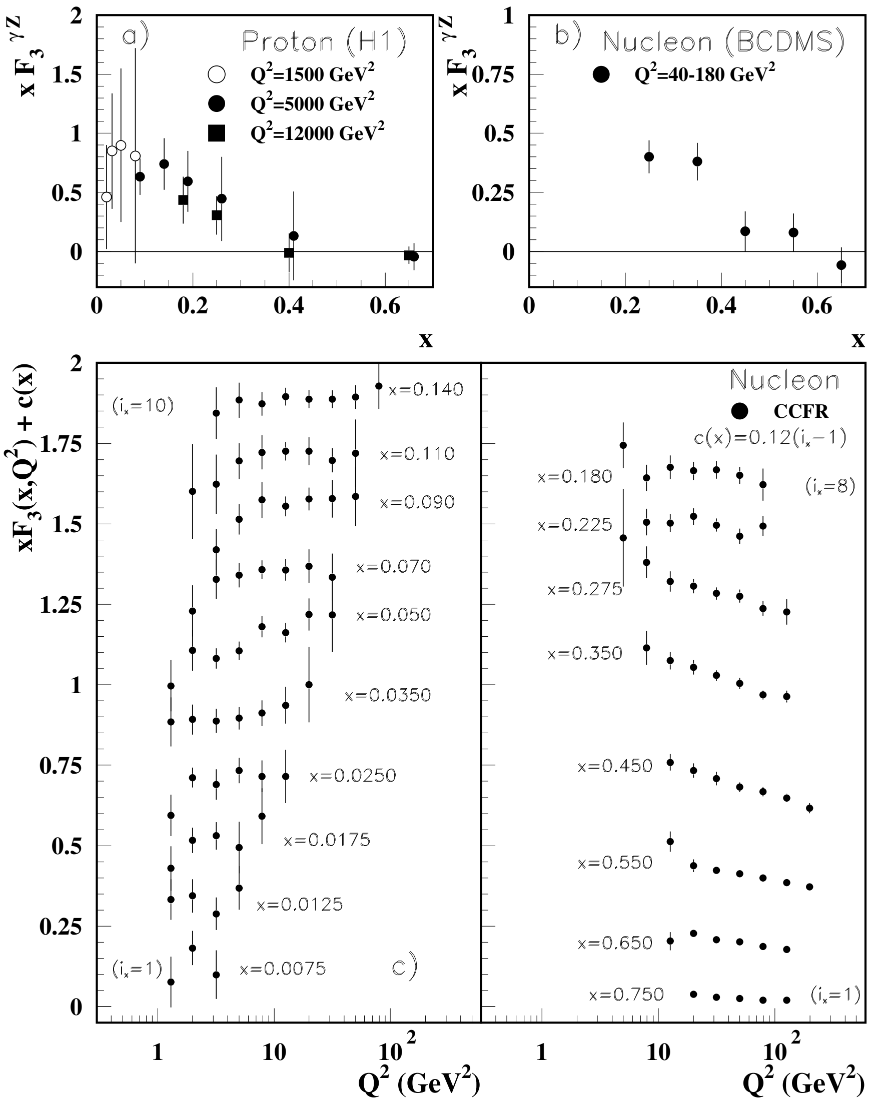

Figure 36.10: The structure function $xF_3^{\gamma Z}$ measured in electroweak scattering of **a)** electrons on protons (H1) and **b)** muons on carbon (BCDMS). Statistical and systematic errors added in quadrature are shown. References: **H1**—C. Adloff *et al.*, Eur. Phys. J. **C19**, 269 (2001); **BCDMS**—A. Argento *et al.*, Phys. Lett. **B140**, 142 (1984).

c) The structure function xF_3 of the nucleon measured in ν-Fe scattering. Statistical and systematic errors added in quadrature are shown. The data are plotted as a function of Q^2 in bins of fixed x. For the purpose of plotting, a constant $c(x) = 0.12(i_x - 1)$ is added to xF_3, where i_x is the number of the x bin as shown in the plot. References: **CCFR**–W. G. Seligman *et al.*, Phys. Rev. Lett. **79**, 1213 (1997).

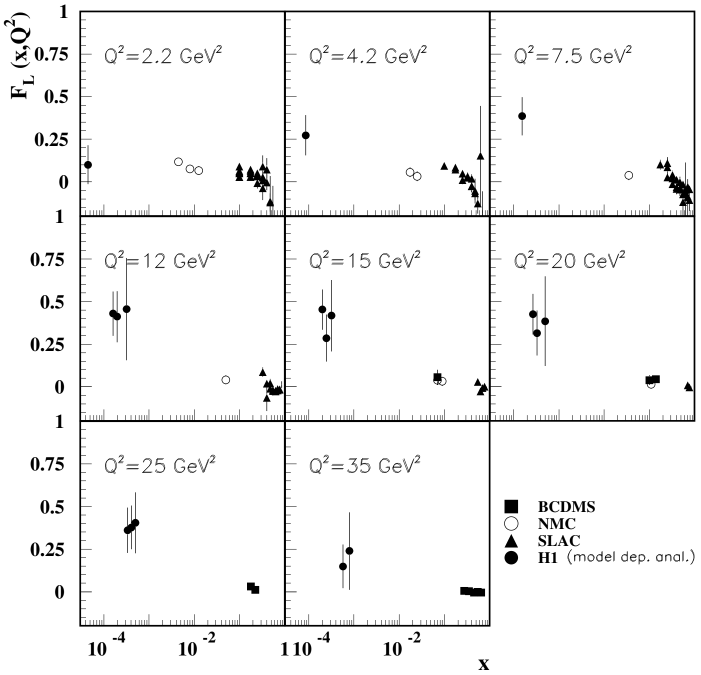

Figure 36.11: The longitudinal structure function F_L as a function of x in bins of fixed Q^2 measured on the proton (except for the SLAC data which also contain deuterium data). The H1 result requires the assumption of the validity of the QCD form for the F_2 structure function in order to extract F_L. BCDMS, NMC, and SLAC results are from measurements of R (the ratio of longitudinal to transverse photon absorption cross sections) which are converted to F_L by using the BDCMS parameterization of F_2 (A.C. Benvenuti *et al.*, Phys. Lett. **B223**, 485 (1989)). It is assumed that the Q^2 dependence of the fix-target data is small within a given Q^2 bin. Statistical and systematic errors added in quadrature are shown. References: **H1**—C. Adloff *et al.*, Eur. Phys. J. **C21**, 33 (2001); **BCDMS**—A. Benvenuti *et al.*, Phys. Lett. **B223**, 485 (1989); **NMC**—M. Arneodo *et al.*, Nucl. Phys. **B483**, 3 (1997); **SLAC**— L.W. Whitlow *et al.*, Phys. Lett. **B250**, 193 (1990) and numerical values from the thesis of L.W. Whitlow (SLAC-357).

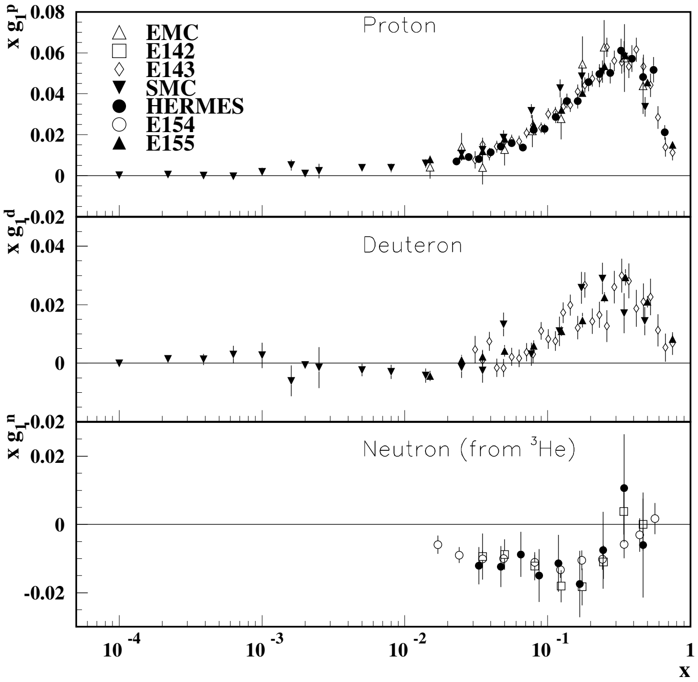

Figure 36.12: The spin-dependent structure function $xg_1(x)$ of the proton, deuteron, and neutron (from ^{3}He target) measured in deep inelastic scattering of polarized electrons/positrons: E142 ($Q^2 \sim 0.3 - 10$ GeV^2), E143 ($Q^2 \sim 0.3 - 10$ GeV^2), E154 ($Q^2 \sim 1 - 17$ GeV^2), E155 ($Q^2 \sim 1 - 40$ GeV^2), HERMES ($Q^2 \sim 0.8 - 20$ GeV^2) and muons: EMC ($Q^2 \sim 1.5 - 100$ GeV^2), SMC ($Q^2 \sim 0.01 - 100$ GeV^2), shown at the measured Q^2 (except for EMC data given $Q^2 = 10.7$ GeV^2 and E155 data given at $Q^2 = 5$ GeV^2). Note that $g_1^n(x)$ may also be extracted by taking the difference between $g_1^d(x)$ and $g_1^p(x)$, but these values have been omitted in the bottom plot for clarity. Statistical and systematic errors added in quadrature are shown. References: **EMC**—J. Ashman *et al.*, Nucl. Phys. **B328**, 1 (1989); **E142**—P.L. Anthony *et al.*, Phys. Rev. **D54**, 6620 (1996); **E143**—K. Abe *et al.*, Phys. Rev. **D58**, 112003 (1998); **SMC**—B. Adeva *et al.*, Phys. Rev. **D58**, 112001 (1998), B. Adeva *et al.*, Phys. Rev. **D60**, 072004 (1999) and Erratum-Phys. Rev. **D62**, 079902 (2000); **HERMES**—A. Airapetian *et al.*, Phys. Lett. **B442**, 484 (1998) and K. Ackerstaff *et al.*, Phys. Lett. **B404**, 383 (1997); **E154**—K. Abe *et al.*, Phys. Rev. Lett. **79**, 26 (1997); **E155**—P.L. Anthony *et al.*, Phys. Lett. **B463**, 339 (1999) and P.L. Anthony *et al.*, Phys. Lett. **B493**, 19 (2000).